Wind-Tunnel Investigation of Vortex Refraction Effects on Aircraft Noise Propagation

R. W. Jeffery,* E. G. Broadbent,† and A. F. Hazell‡
Royal Aircraft Establishment, Farnborough, Hants, England

One possible method for reducing aircraft flyover noise is to site the engines so that the wing vortex can refract sound away from the ground. A series of experiments was carried out in the RAE 24-ft wind tunnel using a model of the HP 115 slender delta research aircraft, which produced a strong leading-edge vortex when set at incidence. The engine noise was simulated by a Hartmann whistle mounted above the engine intake. The results are compared with a theoretical prediction based on ray theory and a simplified representation of the wing vortex structure.

I. Introduction

THE reduction of aircraft flyover noise and of the nuisance to communities living near major airports is a subject of continuing importance. Although considerable benefits have already been achieved from imporvements in engine design and acoustic treatment, further substantial noise reductions below the lowest levels of current aircraft may only be achieved with an acceptable economic penalty if, in addition, new design and operational features that can affect the amount of noise reaching the ground may be efficiently utilized.

Among design features, application of airframe shielding techniques has been shown to be effective for simple localized sources, although for realistic engine noise sources prediction of shielding under flight conditions with reasonable accuracy still presents some difficulties. Another possibility, which is the subject of an idealized study in this paper, is to use the vortex system trailing from the wing to refract the engine noise away from the ground to give noise reduction benefits.

The results presented in this paper are complementary to those of Jeffery and Holbeche.[1] In both cases, experiments were made to measure the noise alleviation due to shielding by the airframe and refraction by the airflow for the Handley Page 115 slender delta research aircraft (Fig. 1) fitted with an intense noise source on top of the engine nacelle. Originally built to provide information on the low-speed handling qualities of a slender-winged aircraft, it subsequently lent itself to acoustic studies through having a relatively simple planform shape amenable to diffraction calculations and a well-defined leading-edge vortex structure which simplified calculation of the effects of vortex refraction.

In the previous work, emphasis was placed on measuring the noise in the shadow region under the aircraft, where there was a substantial noise reduction due to shielding by the delta wing. Measurements were made in flight and at model scale in a wind tunnel and compared with shielding levels predicted by a simple theory based on Cooke's[2] asymptotic approximation to the exact solution for sound diffraction by a half-plane. The accuracy of this approximation under ideal conditions was shown to be good from comparisons with measured sound diffraction around a screen with a straight sharp edge mounted between the walls of an anechoic chamber.

Presented as Paper 76-588 at the 3rd Aero-Acoustics Conference, Palo Alto, Calif., July 20-23, 1976; submitted July 28, 1976; revision received April 12, 1977.

Index categories: Aerodynamics; Noise; Aeroacoustics.

*Senior Scientific Officer, Aerodynamics Department.
†Deputy Chief Scientific Officer, Aerodynamics Department.
‡Scientific Officer, Aerodynamics Department.

Figure 2 is a summary of the shielding results for the HP 115 in flight and wind tunnel compared with a theoretical prediction of diffraction around a half-plane, the edge of which represents the leading edge of the wing nearest to the observer. The variation of noise reduction round the roll plane is plotted with the shadow boundary taken as the origin. All three sets of results show a similar trend in noise reduction inside the shadow of the wing. The predicted shielding for a single edge may be taken as an upper limit since the noise source was mounted close to the centroid of the wing and diffraction took place at three edges rather than one. Noise reductions due to shielding are seen to be substantial, reaching values of up to 20 dB at points well into the shadow region of the wing.

In the previous experiment, no flight and only a limited number of wind-tunnel measurements were made outside the shadow boundary, chiefly because the shadow extends laterally a considerable distance when the aircraft is in a flying attitude with the noise source mounted on the engine nacelle a relatively small distance above the wing. Figure 3 shows results for the previous wind-tunnel experiment with the model mounted at 10° incidence. The line of the microphone traverse was approximately under the noise source, parallel to the wing plane and perpendicular to the flow direction; at its furthest distance from the model the microphone was about 13° outside the wing shadow boundary. The results show a definite flowfield effect outside the shadow that is attributed to the sound being redirected or refracted by the strong leading edge vortex produced on the model at incidence. This effect complements the strong noise reduction due to shielding measured beneath the wing by providing an additional noise reduction of approximately 8 dB in the unshielded region to the side of the aircraft.

Although the evidence for this additional reduction was particularly clear in the wind-tunnel tests, it was also found in earlier flight tests where results were obtained from a single microphone placed outside the wing shadow.[3] The purpose of the present series of experiments was twofold: to investigate noise refraction by the wing vortex in more detail and to provide data for a comparison with theoretical results for refraction by the vortex system of a slender delta wing. The measurements extend further out of the wing shadow than those of the previous experiment in order to cover the whole region in which the sound is influenced by vortex refraction effects.

II. Experimental Details

The experiments were conducted using a ¼-scale model of the HP 115 aircraft in the RAE 24-ft-diam open-jet acoustic wind tunnel.[4] This facility has been acoustically treated to

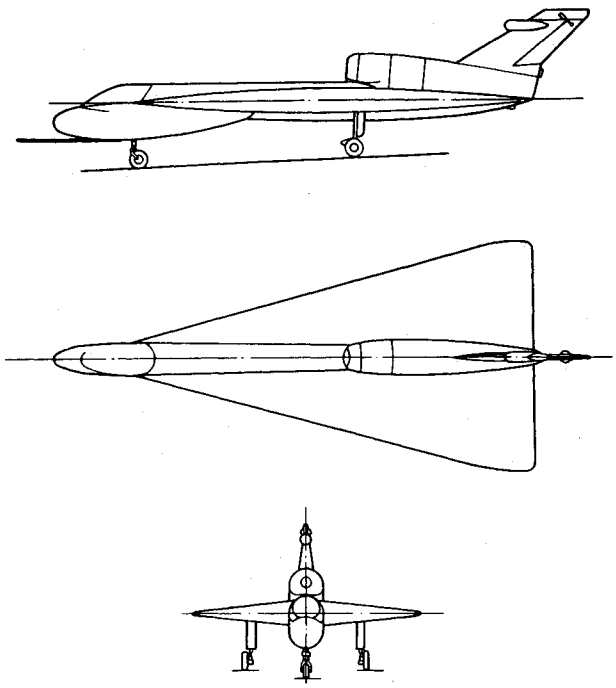

Fig. 1 Handley-Page HP 115.

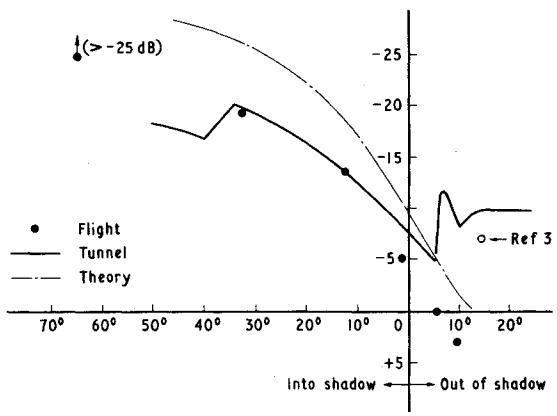

Fig. 2 Comparison of measured shielding with prediction for half-plane.

make it suitable for noise experiments under forward-speed conditions. The experiment was part of a research program to compare measurements of noise reduction from flight and wind tunnel with a theoretical prediction. This particular part of the program, in which measurements were concentrated in the region outside the wing shadow boundary where airflow effects predominate, was not duplicated in flight. But, for the other parts of the program, acoustic similarity between model and full-scale was preserved by using Hartmann generator noise sources with suitably scaled frequencies, 12 kHz for the tunnel tests compared with 3 kHz for flight. Since the effect of source frequency is an important parameter the wind-tunnel experiments were made at three source frequencies: 6 kHz, 9 kHz, and 12 kHz, approximately. Figure 4 shows a frequency spectrum for the model operating in the tunnel with a source frequency around 9 kHz, compared with the background noise level for the empty tunnel at a speed of 120 ft sec.$^{-1}$. Although the model and microphone supports cause an increase in the level of the broadband background noise, the Hartmann source is operating some 40 dB above the tunnel and rig-generated noise. In order to reject unwanted background noise, the microphone signal was processed by a Brüel and Kjaer Heterodyne Analyser with a bandwidth of 316 Hz and tuned to the frequency of the noise source.

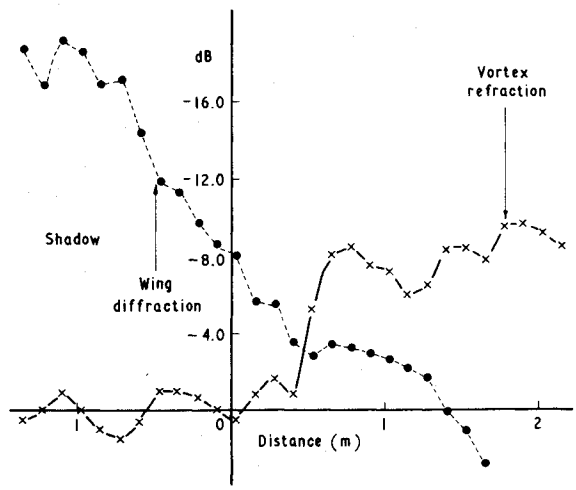

Fig. 3 Total noise reduction at 10° incidence.

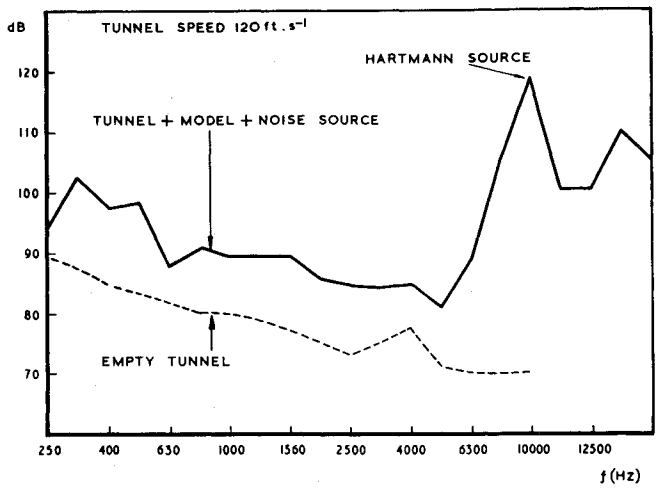

Fig. 4 Tunnel background noise level.

Figure 5 shows the HP 115 model mounted in the 24-ft wind tunnel. To enable the region away from the shadow boundary to be explored in greater detail, the model was mounted on its side in the tunnel working section. The central support column could be rotated on a turntable to alter the model incidence through a range 0°-20°.

The experiments were made by comparing the wind-off noise level, which included diffraction and reflection effects, with the noise level with the tunnel at two different tunnel speeds, 80 ft sec^{-1} and 120 ft sec^{-1}. Microphone traverses were made to the side of the model along directions normal to the zero-incidence plane of the wing at three different streamwise stations: ahead of the model, in line with the noise source, and downstream of the model. In this way, the redistribution of sound in the roll plane was measured as a function of source frequency, model incidence (or vortex strength) with two tunnel speeds over an incidence range 0° -20° in 5° increments, and as a function of streamwise position beneath the model. Sound levels were recorded on a Brüel and Kjaer Level Recorder and refraction effects measured by differencing the wind-off and wind-on records. From these continuous analog records discrete measurements were compared at 32 positions spaced every 5 in. along the microphone traverse. Figure 6 is a schematic representation of the experiment, showing the model and the three different traverse positions.

III. Ray Theory Model for Refraction by a Leading-Edge Vortex

The acoustic intensity is to be computed at the measuring stations by means of ray theory. The cases of interest do not

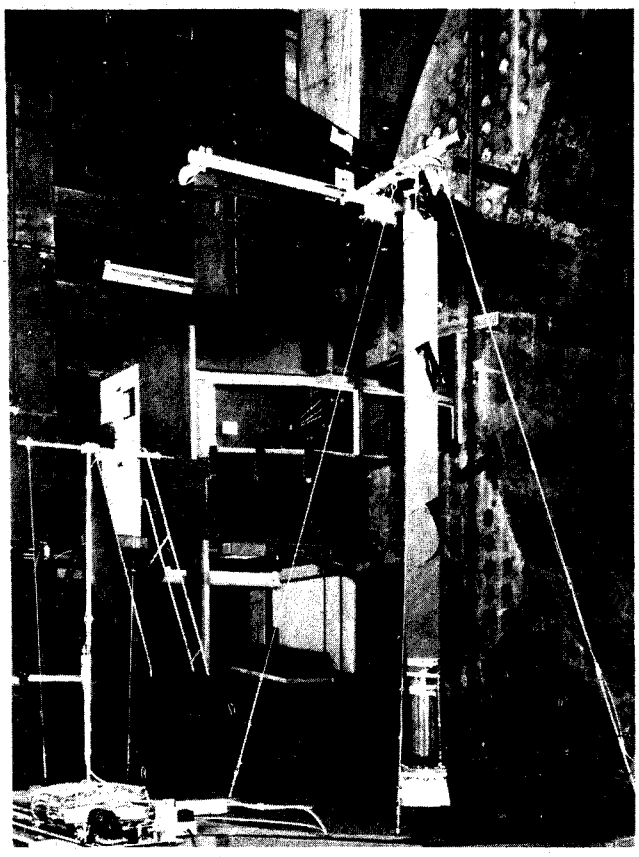

Fig. 5 HP 115 in 24-ft wind tunnel.

involve diffraction, since the measuring points lie outside the wing shadow, but they do involve refraction by the flowfield (in particular by the leading-edge vortices), and they also involve reflection from the wing which can be taken into account by including the image of the source in the wing upper surface.

For ray theory to be valid it is necessary that $kl \gg 1$, where k is the wave number and l is a typical length scale of the flowfield, i.e., a distance over which the velocity changes significantly. On the other hand, ray theory often gives a satisfactory result even when it is not strictly valid; for example, it will predict the correct angle of turn of an incident wave that is refracted at a vortex sheet, although it will ignore any reflections there. In the present examples, k lies in the range 114-228 m^{-1} and the vortex radius in the range 0-0.2 m (based on Ref. 5), so that if l is identified with the vortex radius, then the required condition is satisfied by a reasonable margin except near the wing apex. Within the vortex structure, however, the flow gradients are large so that locally ray theory will be invalid (or at best only marginally valid), but by analogy with the behavior at a vortex sheet it is hoped that the resultant errors will be small.

The vortex structure can, in fact, be closely represented by a rolled-up vortex sheet as calculated for example by Smith.[5] In the present calculations, the size, location, and strength of the vortices are taken from Smith's paper for the appropriate geometric parameters, and these values are assumed to hold between the wing apex and the trailing edge. Right-handed rectangular axes are used, with z in the direction of the freestream and y upward. The slender strip-theory approximation is then used; i.e., the flowfield in a plane z = constant is determined entirely by the vortex structure in that plane.

The velocity profile within the vortex is based on Earnshaw's measurements,[6] but it is made axisymmetric for convenience, since the departures from axisymmetry are small. It is also convenient to have analytic forms for the velocity components. Here we assume the speed of sound, c, to be constant and use nondimensional velocity components (U, V, W) based on that speed; i.e., U is the Mach number of the x component of velocity; also V_θ is the azimuthal component. Then

$$V_\theta = aV_c(\sin b\eta)^q \qquad (\eta \le 1) \tag{1}$$

$$V_\theta = V_c/\eta \qquad (\eta \ge 1) \tag{2}$$

are the formulae used for the flowfield about each leading-edge vortex in a plane z = constant. Here $\eta = r/r_l$ where r_l is the radius of the vortex and r is the distance (in the plane) of a point from its axis; a, b, and q are nondimensional constants and V_c is determined for given geometry (including incidence) from Ref. 5. The constant q was chosen to give roughly the correct profile (based on Ref. 6), and then a and b are defined by the condition that V_θ and its first derivative should be continuous at $\eta = 1$. The result is

$$q = 0.0625 \qquad a = 1.112 \qquad b = 2.96 \tag{3}$$

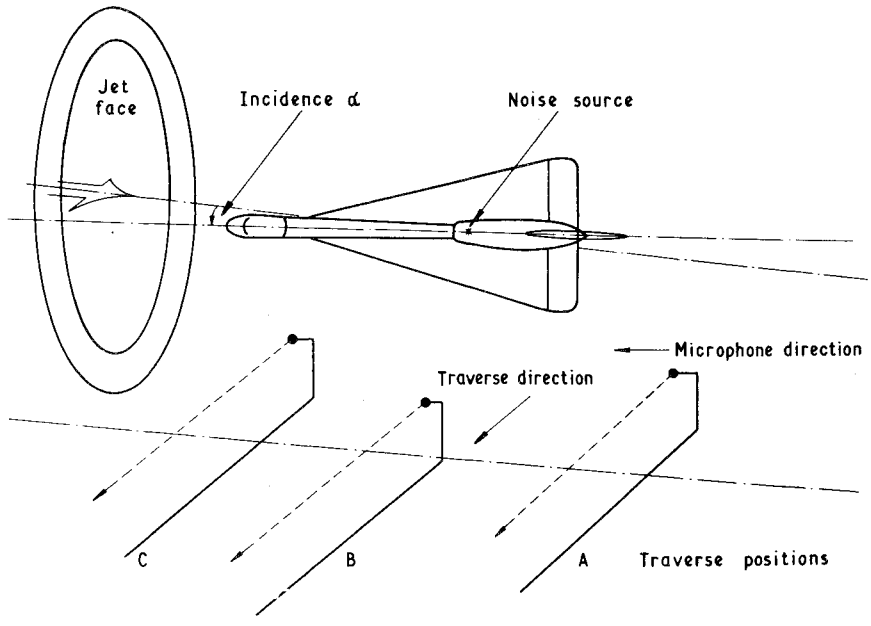

Fig. 6 Schematic of model and traverse.

Linear dimensions are also made nondimensional in the form $X=x/ct_0$, where t_0 is a constant with dimensions of time and is chosen for numerical convenience. The position of the vortex center is then assumed to be given by

$$\left.\begin{aligned} X_v &= B_v(Z-Z_A) \\ Y_v &= Y_A-(Z-Z_A)A_v \end{aligned}\right\} \quad (Z_A\le Z\le Z_T) \qquad (4)$$

where the suffix v denotes the vortex center, the suffix A the apex, and the suffix T the trailing edge. Thus A_v is the incidence of the plane of vortex centers to the freestream, and B_v is the semiangle contained by the vortex centers, on the assumption that both are small constants that depend on geometry.

Behind the trailing edge, it is assumed that the vortex drifts with increasing z until its axis is parallel to the freestream:

$$\left.\begin{aligned} X_v &= B_v(Z_T-Z_A)+\frac{B_v}{B_{v2}}\{1-e^{(Z_T-Z)B_{v2}}\} \\ Y_v &= Y_A-A_v(Z_T-Z_A)-\frac{A_v}{A_{v2}}\{1-e^{(Z_T-Z)A_{v2}}\} \end{aligned}\right\} (Z\ge Z_T) \qquad (5)$$

The radius of the vortex is assumed to increase linearly with Z for $Z<Z_T$ and then to grow parabolically for $Z>Z_T$ such that the slope is continuous at $Z=Z_T$. Thus

$$\begin{aligned} R_l &= B_R(Z-Z_A) \qquad (Z\le Z_T) \\ R_l &= B_{R2}(Z-Z_{A2})^{1/2} \qquad (Z\ge Z_T) \\ Z_{A2} &= \tfrac{1}{2}(Z_T+Z_A) \\ B_{R2} &= \{B_R 2(Z_T-Z_A)\}^{1/2} \end{aligned} \qquad (6)$$

The coefficient B_R can be estimated from Ref. 5, but the exponential coefficients A_{v2} and B_{v2} have been guessed at a reciprocal chord length; they are not important in the present geometry.

The azimuthal velocity distribution is assumed to be independent of Z. This would clearly be unsatisfactory for Z much greater than Z_T, but this does not apply with the measuring positions used in the experiment. Near the wing surface, the assumption of axisymmetry must also be seriously wrong, but rays close to the surface are in any case difficult to treat accurately, because of the combined effects of refraction and diffraction. The best one can do for the diffracted field with the present model is to calculate the refracted rays that illuminate the leading edge, and their intensity at the edge, and then to deal with diffraction by a standard method (see, e.g., Ref. 7).

In addition to the azimuthal velocity within the vortex, there is also an axial distribution. This has again been used on the measured results of Earnshaw[7] and an approximate analytic form derived.

$$\begin{aligned} W &= W_0\left\{1+W_p\left(\cos\frac{\pi}{2}\eta\right)^{n_w}\right\} \qquad (\eta\le 1) \\ &= W_0 \qquad (\eta\ge 1) \end{aligned} \qquad (7)$$

Numerical values for the constants were chosen to be

$$\begin{aligned} W_p &= W_{p0}=2.9V_c/W_0 \qquad (Z_A\le Z\le Z_T) \\ n_w &= 8 \end{aligned} \qquad (8)$$

For $Z>Z_T$ we assume that the axial velocity decays exponentially,

$$W_p = W_{p0}\exp\{W_{p2}(Z_T-Z)\} \qquad (Z\ge Z_T) \qquad (9)$$

where W_{p2} is a further empirical constant of little importance in the present comparisons with experiment.

The equations of ray theory[8] are, with $T=t/t_0$

$$\begin{aligned} \frac{dX}{dT} &= U+F/K \\ \frac{dY}{dT} &= V+G/K \\ \frac{dZ}{dT} &= W+H/K \\ \frac{dF}{dT} &= -F\frac{\partial U}{\partial X}-G\frac{\partial V}{\partial X}-H\frac{\partial W}{\partial X} \\ \frac{dG}{dT} &= -F\frac{\partial U}{\partial Y}-G\frac{\partial V}{\partial Y}-H\frac{\partial W}{\partial Y} \\ \frac{dH}{dT} &= -F\frac{\partial U}{\partial Z}-G\frac{\partial V}{\partial Z}-H\frac{\partial W}{\partial Z} \end{aligned} \qquad (10)$$

with $K\equiv(F,G,H)$, the wave number vector. F,G,H, and K are nondimensional, and since we are only interested in relative values, we take $K=1$ initially.

In the experiments, traverses were carried out with a microphone for which Y was varied at constant X and Z. By a suitable choice of spherical polar coordinates (R,θ,ϕ) with origin at the acoustic source, this traverse can be arranged to correspond with a variation in θ for fixed ϕ. The method of calculation is to integrate Eq. (10) using a fourth order Runge-Kutta procedure and for each ray tube the appropriate conservation laws satisfied (see Ref. 8). Rays from the image source can be treated in the same way. For a fixed frequency (or a fixed narrow-band Fourier component) the acoustic pressures arriving at a given point may be added with due regard to phase (which is known from the elapsed time T and the frequency of the source) to obtain the complete signal at that point. In general, interference fringes will be found in this way. To a lower level of approximation, which may be sufficient in many experiments, the intensities may be added without regard to phase since, on average, energy is conserved.

For a directional source the strength of each ray is determined by the known source characteristics. If these are measured in still air, it is necessary to correct the direction of a ray to obtain corresponding ray intensities with and without flow: if l_0 is the direction of a ray with no flow and l the direction of the corresponding ray with flow, then

$$l=(l_0+V)/(|l_0+V|) \qquad (11)$$

but this makes no allowance for the possible change in the nature of the source resulting from the flow. An alternative is to calibrate the source in a uniform stream. In the present experiments, the characteristics of the source were sufficiently uniform and the flow speed sufficiently low for this correction to be negligible. In particular, the comparative experimental results with and without flow for the wing at zero incidence show differences of no more than experimental scatter at the microphone positions. It should be noted that this includes both any change in the source characteristics by the flow as well as any convective amplification effects.

IV. Wind-Tunnel Results

The effect of airflow on redistributing sound has been measured by differencing the wind-on and wind-off data taken from the microphone traverse. By this process, the static shielding effects, which are appreciable in the wing shadow region, are canceled out. For a discussion of the

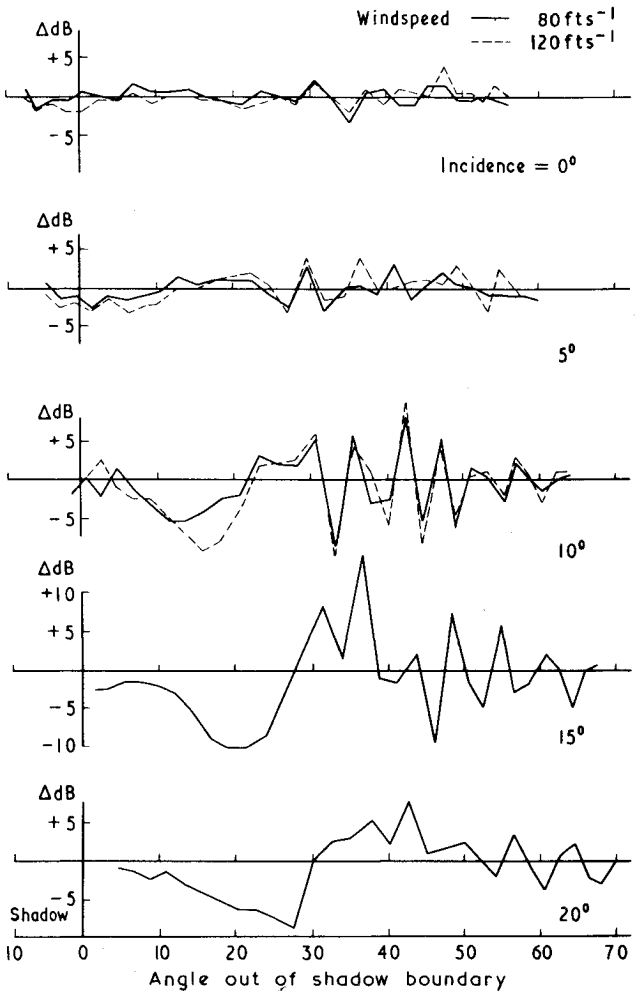

Fig. 7 Noise changes due to airflow. Windspeed: (——) 80 ft/sec; (---) 120 ft/sec. Position A, 6.5 kHz.

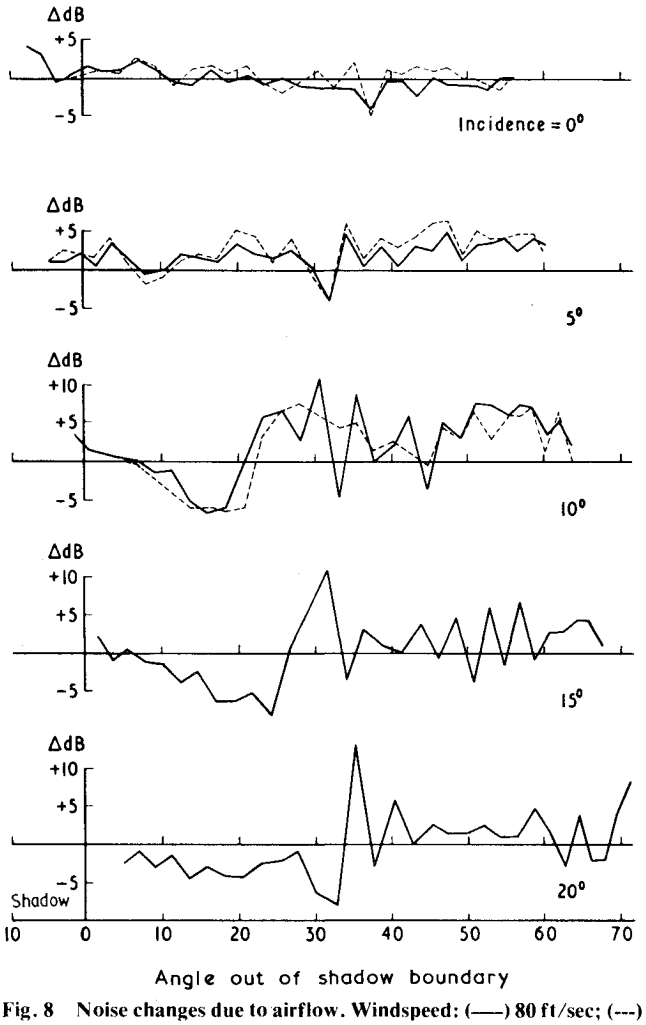

Fig. 8 Noise changes due to airflow. Windspeed: (——) 80 ft/sec; (---) 120 ft/sec. Position A, 9 kHz.

combined effects of vortex refraction and shielding, see Jeffery and Holbeche.[1]

Several assumptions are implicit in this simple differencing of wind-on and wind-off results. Over the range of the experiments, the effects of convection by the tunnel stream are assumed negligible, the source is assumed to be effectively omnidirectional, and its characteristics are assumed not to be influenced by the tunnel flow. The justification for these assumptions may be seen in the differenced results presented for 0° incidence (Figs. 7-13) where, in the absence of any vortex structure, the flow effects are small. These zero-incidence traverses are, in fact, taken as an indication of the likely accuracy of this simplified method of data analysis over the entire range of the experiment.

Figures 7-9 show the results for position A (behind the model), Figs. 10-12 for position C (ahead of the model), and Fig. 13 for position B (nearly under the noise source). For positions A and C data is presented for three source frequencies, 6 kHz, 9 kHz, and 12 kHz. For position B only one source frequency is shown, because, as explained below, data is only available for a region which is strongly influenced by reflections from the wing surface and where no overall noise reduction due to refraction effects was found. For positions A and C, however, data is for an incidence range from 0° to 20° in 5° increments with a tunnel speed of 80 ft sec^{-1} and from 0° to 10° at 120 ft sec^{-1} (because of a loading limitation on the model support column).

The microphone position along the traverse is shown as the angle into or out of the shadow, the angle being that between the lines joining the source to the microphone and to the line from source to microphone which touches the wing leading edge, measured in the plane containing the source and the traversed line. Reflections from the surface of the wing and nacelle are expected at points outside the wing shadow, for position A, behind the model. Fewer points are in shadow as the incidence increases, but for position C more points lie in the wing shadow as incidence is increased.

The general character of the figures is the same for all three frequencies and traverse positions. The difference between wind-on and wind-off is small at 0° incidence but becomes increasingly pronounced and develops into a characteristic pattern as incidence is increased. In the region just outside the shadow boundary, where the sound is influenced by passage through the wing vortex, there is a progressive reduction in sound level as incidence increases. To the right of the figures, in the region where the microphone receives a strong reflected signal from the wing as well as a signal directly from the source, a "peaky" pattern develops, which we attribute to interference between these two signals. These two features are discussed in turn.

In the earlier work, for a traverse position under the noise source, little sound reduction due to refraction was measured until the observer was 5° or more outside the shadow boundary. Figures 7-9, for position A behind the model, also show no reduction due to refraction for points in the shadow boundary but rather a buildup starting at about 5° to 10° reaching a maximum some 15° to 20° outside the shadow boundary. This is in agreement with the earlier work. However, at position C, Figs. 10-12, the maximum effect is found much closer to the shadow boundary and the effect begins to build up actually in the shadow of the wing, a reduction of some 5 dB being measured at the boundary.

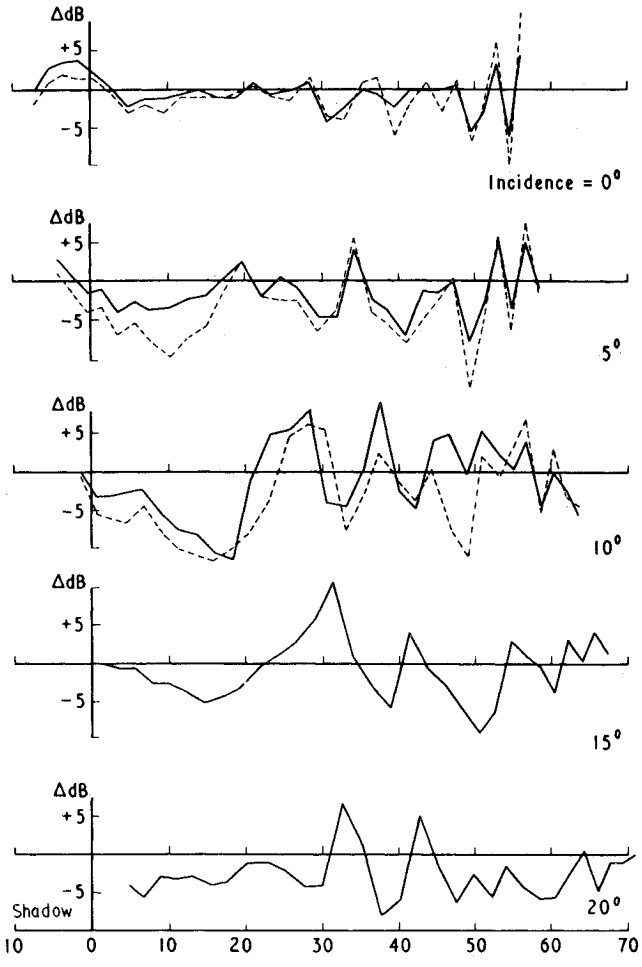

Fig. 9 Noise changes due to airflow. Windspeed: (——) 80 ft/sec; (---) 120 ft/sec. Position A, 12.5 kHz.

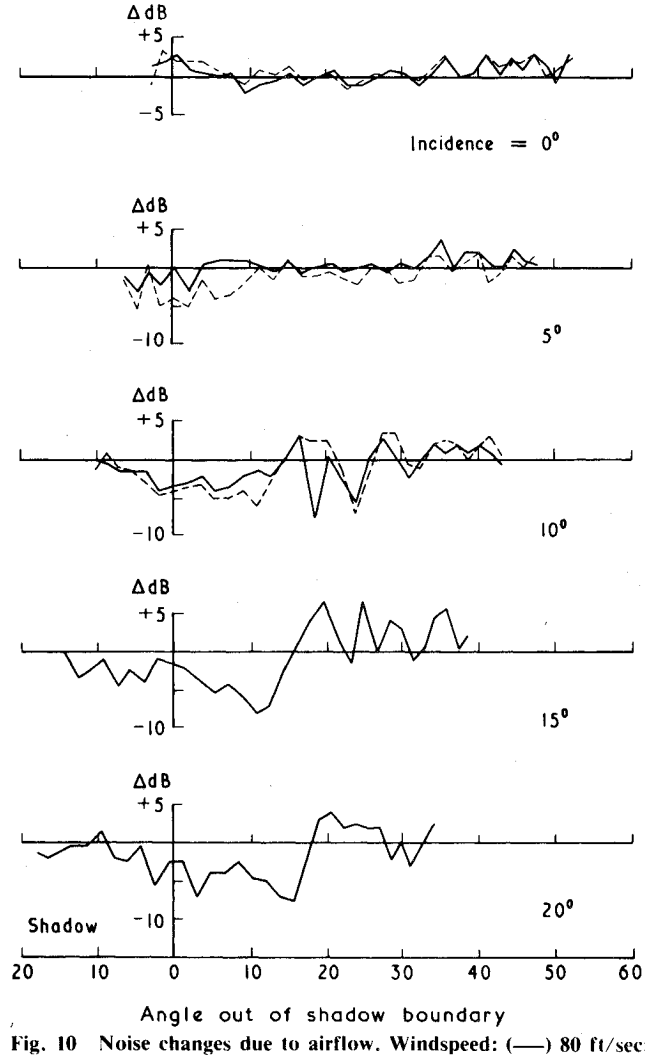

Fig. 10 Noise changes due to airflow. Windspeed: (——) 80 ft/sec; (---) 120 ft/sec. Position C, 6.7 kHz.

For position A, noise reduction of between 5 and 12.5 dB are found for three different source frequencies at 10° and 15° incidence with tunnel speeds of 80 ft sec^{-1} and 120 ft sec^{-1}. The noise reduction is more pronounced at the higher tunnel speed, (although the reflection patterns to the right of the figures do not vary systematically with different tunnel speeds). For this traverse, the noise reduction is not so great at 20° incidence as for 10° or 15°, but at this high incidence the greatest reduction is for the low-frequency noise source. The sound reduction is frequency dependent, but for a fixed incidence this reduction may either increase or decrease with frequency. For position A, the maximum effect occurs about 20° outside the shadow boundary. The position of peak noise reduction moves further out from the shadow boundary as the model incidence increases, consistent with the movement of the vortex core further from the wing at higher incidence.

Zero incidence results for all traverse positions suggest that the source is less well behaved at high frequency than at the other two lower frequencies. However, this deterioration shows up mainly in the region influenced by wing reflections; in the region of sound reduction by the vortex, the behavior at high frequencies remains tolerably good.

For traverse position C, the significant noise reductions are in a shadow region closer to the shadow boundary than for position A, and there is not, in this case, a fall-off at 20° incidence, the reduction being about the same (or greater, for the high-frequency source) as at 10° or 15° incidence. In general, the noise reductions are not so great as for position A, being between 5 and 10 dB. The observation that the noise reductions are closer to the wing shadow for position C, ahead of the model, is consistent with the fact that for a slender delta wing leading-edge vortex, the core is closer to the wing surface near the wing apex. In other respects the results for position C are similar to position A; the results are frequency dependent for a given incidence, and the reflections are little affected by tunnel speeds. The position of the reduction peak moves out from the shadow boundary with increased incidence.

For position B (Fig. 13), the end of the traverse was placed against the central model support column and, since the microphone stopped some distance before this point, data are not available on the shadow side of the wing. However, data from this traverse position do show the marked peaks and troughs that occur over the main region of interference between direct sound and sound reflected from the wing or nacelle surface. This effect, which is so marked in the present results because a monochromatic sound source has been used, is more clearly illustrated in Fig. 14, which shows the continuous traces from the level recorder for wind-off and wind-on at a source frequency of 6.3 kHz. For wind-off, the traces for all angles of incidence are similar in showing a pattern of successive reinforcement and cancellation, which is particularly pronounced in the segment from about 30° to 60° out of the shadow where there is a strong reflected field from the wing. In a zero-lift condition, this pattern is unaffected by airflow, the level recorder traces for the model at zero incidence with wind-on and wind-off, being almost identical. This is perhaps the clearest evidence in the present work that the Hartmann source was not significantly affected by the flow and that convective amplification was, as expected, small.

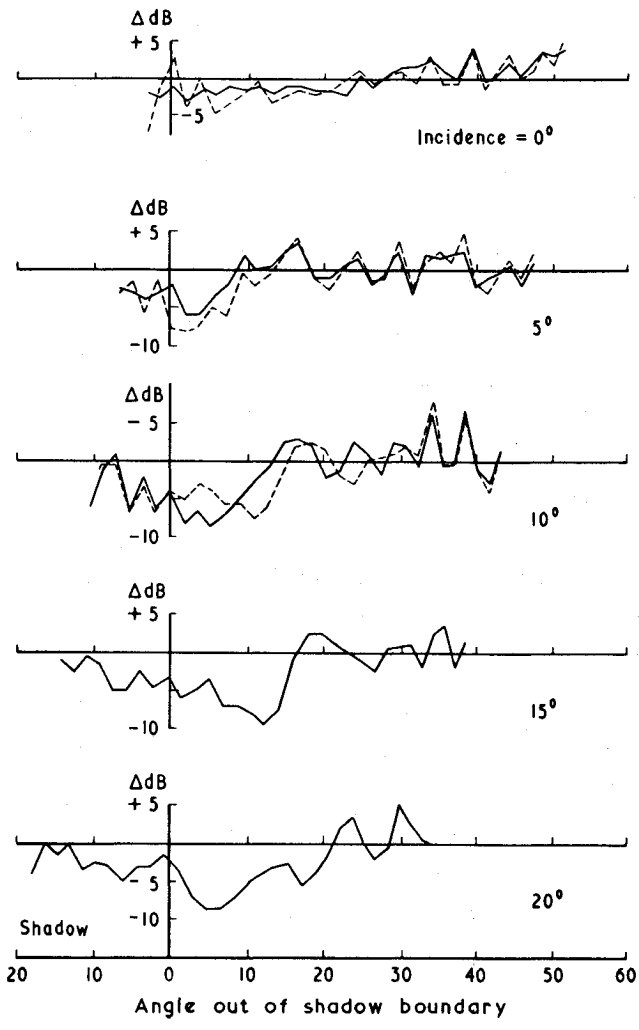

Fig. 11 Noise changes due to airflow. Windspeed: (——) 80 ft/sec; (---) 120 ft/sec. Position C, 9.7 kHz.

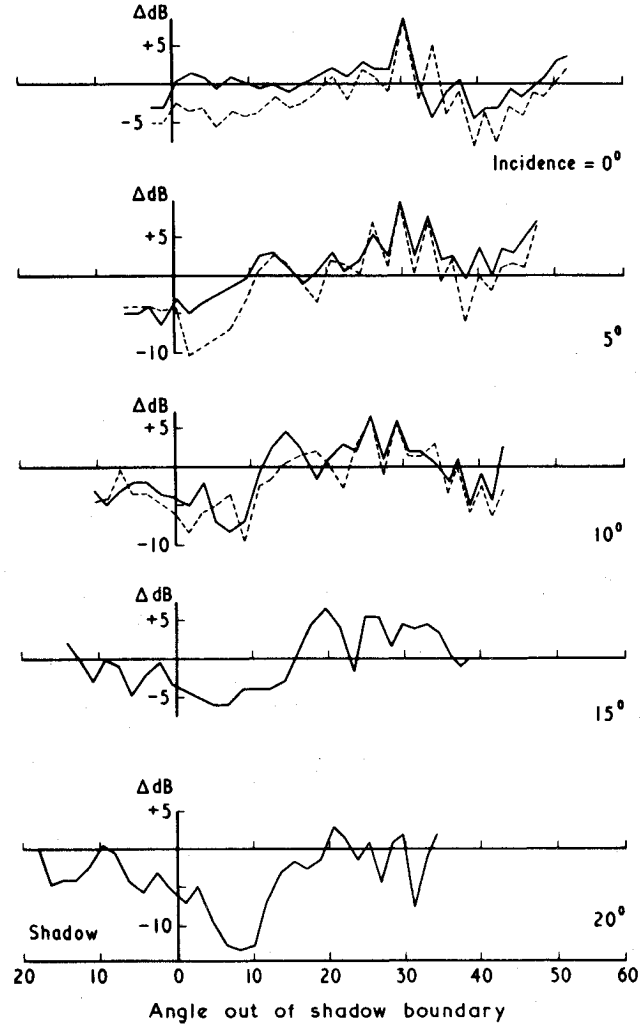

Fig. 12 Noise changes due to airflow. Windspeed: (——) 80 ft/sec; (---) 120 ft/sec. Position C, 12.8 kHz.

Similar data, with the model at 10° incidence show that the static reflection pattern is similar but has been shifted laterally due to rotation of the wing surface through the incidence angle. Comparing wind-on and wind-off reflections at 10° incidence, it can be seen that the same fundamental pattern has been shifted and also distorted by the airflow. This shift of a rapidly changing sound picture means that the present data analysis, in which wind-off and wind-on noise levels are differenced at a set of discrete points along the traverse leads to a peakiness in Figs. 7-13 in the region where there are strong reflections from the wing. For the model at 15° incidence, the effect on the reflection pattern has also increased, the shift and distortion being appreciably greater than for 10° incidence. The inference drawn from these graphs is that the interference pattern between the direct and reflected sound is changed by the leading-edge vortex as a result of changes in the path lengths of interfering rays due to their passage through the rotating flow. Although this phenomena is discussed in relation to traverse position B, the effect is seen for all frequencies and for each traverse position.

At higher source frequencies, the sound level differences are even more peaky since the basic reflection patterns are more condensed, and so a smaller shift due to airflow effects is sufficient to produce large differences.

Figures 15 and 16 illustrate the manner in which sound has been redistributed by the airflow. Figure 15 compares the level recorder traces wind-on and wind-off, for the downstream position A. At 15° incidence, a large amount of sound is missing in the region to the left of the graph where the direct line from source to microphone passes through the vortex. Since the sound has been refracted upward by the vortex, we may expect the deficit in the left-hand side of the figure to be offset by an increased level to the right. This effect is clearly apparent at 15° incidence; it is also noticeable that outside this region of sound redistribution the reflection pattern has been shifted by the airflow effects, as was seen at traverse position B. Also on Fig. 15 the results at 20° incidence are shown. Although sound is again missing from the initial part of the microphone traverse, it does not reappear to so great an extent further along the traverse. In both cases the source frequency is 6.5 kHz.

Figure 16 shows similar results for the upstream traverse position C, with a source frequency of 12.8 kHz and aircraft incidence of 10° and 20°. At 10° incidence sound is redistributed along the microphone traverse, as found for traverse position A. But at 20° incidence and again in keeping with position A, there is a large net sound deficit. So, it would appear that the effect of refraction by the vortex system is not simply a vertical redistribution of energy but may also include a significant longitudinal redistribution, possibly due to the strong gradients of axial velocity within the vortex. However, since measurements were not made at sufficiently close longitudinal spacing, this suggestion cannot be substantiated.

As outlined in Sec. III previously, ray theory has been used to calculate acoustic intensities at the position of traverse C for the wing at 15° incidence. A comparison with the observations is shown in Fig. 17, covering a range of 30° away from the shadow boundary. There is a general qualitative agreement between the two curves, in that both show a region of noise reduction between 2° and 14°, and the magnitude of

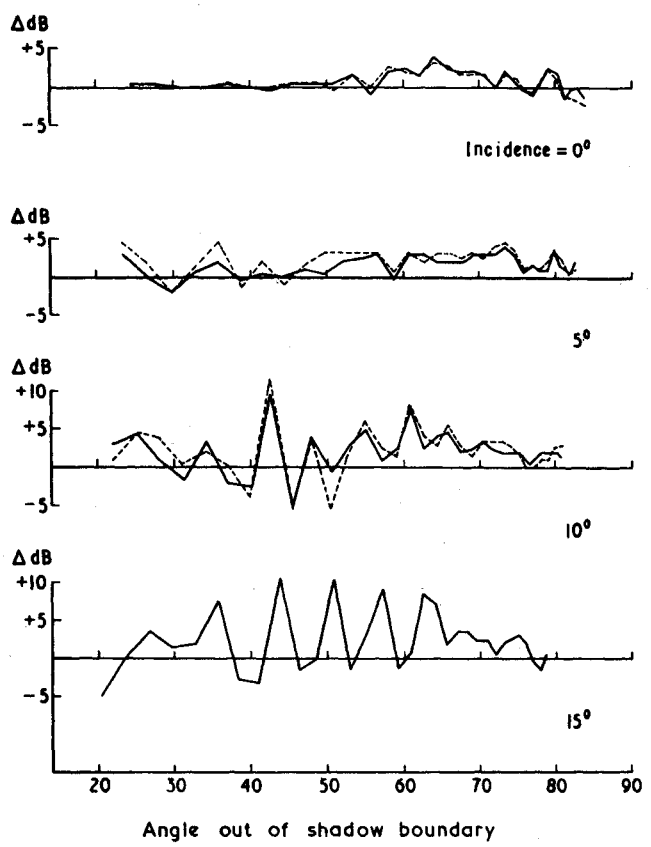

Fig. 13 Noise changes due to airflow. Windspeed: (——) 80 ft/sec; (---) 120 ft/sec. Position B, 6.3 kHz.

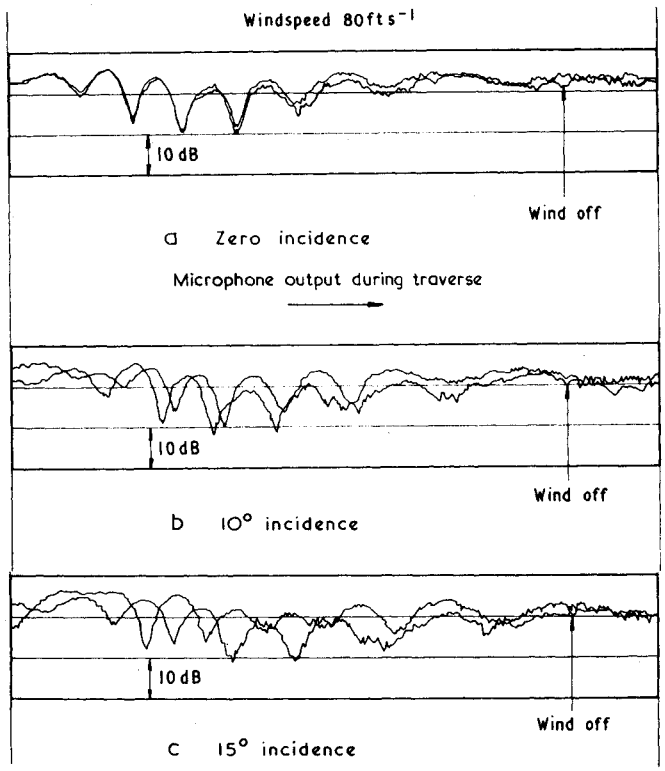

Fig. 14 Position B. Airflow effects on reflections.

the reduction is the same to within approximately 1 dB or so; both also show a region of noise increase for angles greater than about 20° with a dip in the middle. On the other hand, ray theory shows additional positive spikes (focusing) that are not matched by the observations. The spike near 0° would, in practice, be greatly modified both by the flow near the surface

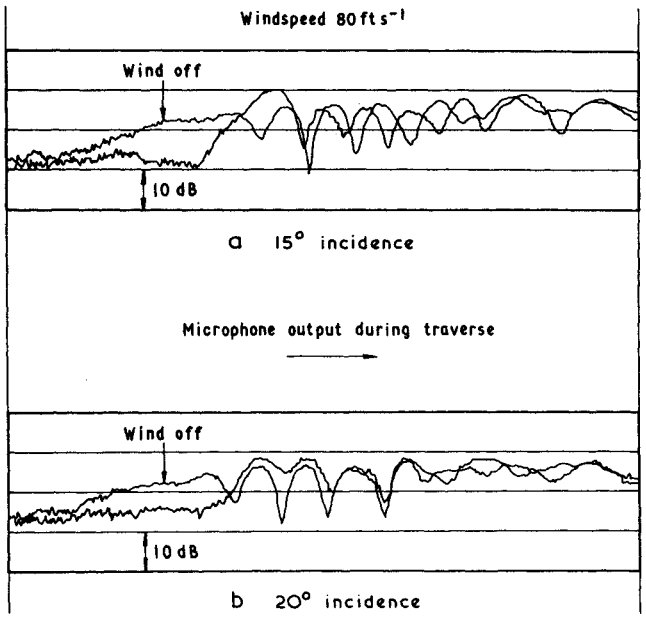

Fig. 15 Position A. Sound redistribution by airflow.

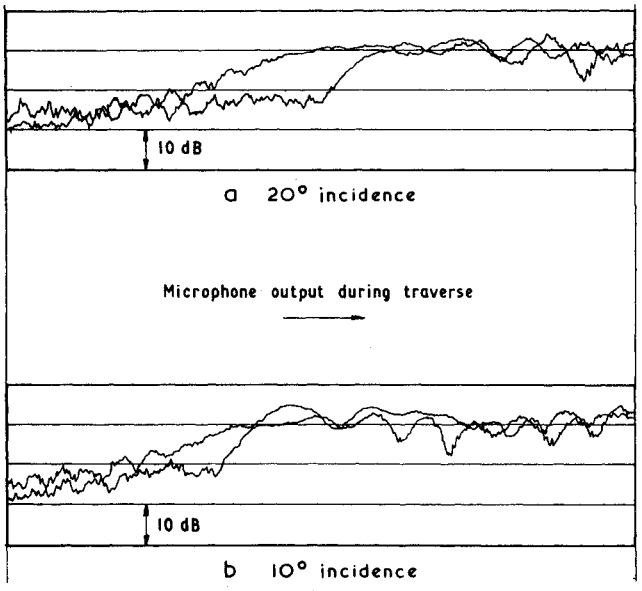

Fig. 16 Position C.

(which is incorrectly represented by the mathematical model) and by diffraction at the leading edge. The reason for the spike near to 15° is not clear and further calculations are in hand on this point. Ray theory becomes invalid in the region of a caustic (although it can be used again beyond the caustic where the ray tube in question has regained a finite size) so that the absolute magnitude of the ray-theory spikes are exaggerated and, in the limit, meaningless; they are therefore shown as open-ended in Fig. 17.

The comparison is made for 12.8 kHz for which the criterion $kl \gg 1$ (see Sec. III) is best satisfied. Since only first-order ray theory was used, the calculated curve is independent of frequency, subject to $kl \gg 1$ and in the absence of interference effects (see below), although the experimental results do change somewhat over the frequency range covered as may be seen from Figs. 10-12. Nevertheless, the main feature of both the calculated and experimental results is the range of reduced noise, which for 15° incidence occurs at angles of up to approximately 15° out of shadow. This angular range remains remarkably constant over the frequency range tested and agrees reasonably well with that obtained from calculations; the detailed shape of the curve is

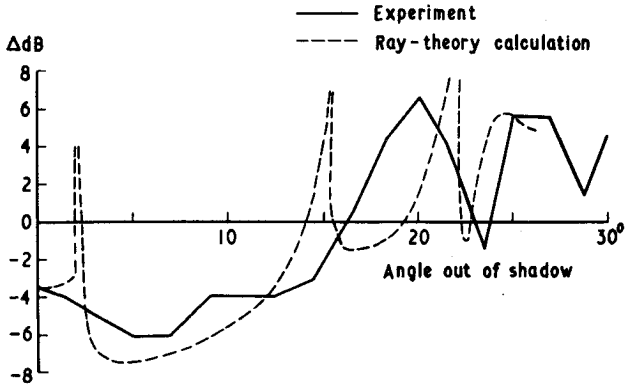

Fig. 17 Position C, 15° incidence. Ray theory calculation.

not well predicted by the calculations and becomes somewhat less so at the lowest test frequency.

Some rays from the image source were calculated, but they do not interact over the range shown. This result, however, is based on the approximation that the wing upper surface is flat, whereas the true upper surface has slight curvature which will increase the angular range of the reflected rays somewhat. Even so, there should be little effect at angles within 30° of the shadow boundary.

V. Conclusions

Experiments in the RAE 24-ft wind tunnel, using a ¼-scale model of the HP 115 slender delta research aircraft with a noise source mounted centrally above the wing, have shown the leading-edge vortices of this type of wing to have a pronounced influence on the far-field noise distribution.

The primary effect is that the sound passing through the core region of the vortex is refracted upward, with the result that sound intensities in the far-field are greatly reduced along lines of sight from the source through the vortex. In effect, there is a shadow region beyond the vortex, the size and intensity of which will depend on the strength of the vortex, the distance from vortex to source, and the scale of the vortex relative to the acoustic wavelength. In the present experiments, a sound reduction in excess of 10 dB was observed at the highest wing incidence and source frequency. Although the vortex structure on a slender-wing aircraft differs appreciably from that of a conventional, swept-wing aircraft, these results suggest that, for the latter case also, vortex refraction effects could have a significant effect on the far-field noise.

The second observed effect was a modification of the pronounced interference pattern produced in the region where there were both direct waves from the monochromatic sound source and waves reflected from the wing upper surface. This pattern was not influenced by tunnel flow when the model was at zero lift but was shifted and distorted when the wing was at incidence, presumably as a result of changes in the path length (and hence phase) of the interfering rays brought about by their passage through the vortex flowfield.

A method for predicting both effects using ray theory is described and a sample calculation of the sound field in the reflection-free region is shown. The predicted depth and extent of the vortex shadow agrees broadly with experiment, although some additional positive spikes are predicted that need further examination.

References

[1] Jeffery, R. W. and Holbeche, T. A., "An Experimental Investigation of Noise-Shielding Effects for a Delta-Winged Aircraft in Flight, Wind Tunnel and Anechoic Room," *Progress in Astronautics and Aeronautics*, Vol. 45, edited by I. R. Schwartz, AIAA, New York, 1976.

[2] Cooke, J. C., "Notes on the Diffraction of Sound," RAE Tech. Rept. 69283, 1969.

[3] Broadbent, E. G., Holbeche, T. A., and Butler, G. F., "Interaction of a Vortex Core with Acoustic Radiation," Euromech 34, *Control and Feedback Mechanisms in Flow Noise*, Göttingen, Sept. 1972.

[4] Holbeche, T. A. and Williams, J., "Acoustic Considerations for Noise Experiments at Model Scale in Subsonic Wind Tunnels," RAE Tech. Rept. 72155, 1972.

[5] Smith, J.H.B., "Improved Calculations of Leading Edge Separation from Slender, Thin, Delta Wings," *Proceedings of the Royal Society*, A 306, 1968, pp. 67-90.

[6] Earnshaw, P. B., "An Experimental Investigation of the Structure of a Leading Edge Vortex," British ARC, R&M 3281, 1961.

[7] Broadbent, E. G., "Noise Shielding for Aircraft," RAE Tech. Rept. 76002, 1976.

[8] Lighthill, M. J., "The Propagation of Sound Through Moving Fluids," *Journal of Sound and Vibration Research*, Vol. 24, 1972, p. 471.